Determination of vehicle loads on bridges by acoustic emission and an improved ensemble artificial neural network

Laxman K C [a], Allen Ross [a], Li Ai [a,*], Alexander Henderson [a], Elhussien Elbatanouny [a], Mahmoud Bayat [a], Paul Ziehl [a,b]

[a] Department of Civil and Environmental Engineering, University of South Carolina, Columbia, SC, USA
[b] Department of Mechanical Engineering, University of South Carolina, Columbia, SC, USA

ARTICLE INFO

ABSTRACT

Bridges are significant hubs in the U.S. national economy, facilitating the movement of goods and vehicles. The condition of bridges in the state of South Carolina is currently under scrutiny, especially in rural areas where most of the bridges were designed using outdated standards from the 1950 s. The weight of vehicles in recent years has increased significantly compared to the past. This has created an overloading problem. In addition, bridge performance decreases during their service life due to vehicle loads, material deterioration, and environmental erosion. Therefore, it is necessary to inspect and conduct load ratings on bridges to determine whether the bridges need to be posted. Due to recent advances in sensing technology and data analysis methods, nondestructive methods such as acoustic emission (AE) have been widely utilized in monitoring damage to the bridges. The objective of this paper is to explore the possibility of using AE sensors concurrently to determine vehicle loads on the bridges while monitoring bridge damage. A load determination method leveraging an improved ensemble artificial neural network (ANN) is proposed to analyze the AE data and estimate the load of the vehicle. The significance of this vehicle load determination method is that it has the potential to be paired with an AE damage monitoring system rather than using other instrumentation such as a weigh-in-motion (WIM) system. The proposed method has been tested on an experimental bridge component. The results suggest that the proposed model has an accuracy above 70 % in estimating the vehicle loads on the precast reinforced concrete (RC) flat slabs.

1. Introduction

South Carolina depends heavily on its numerous bridges for community connectedness, trade, and transportation. The state has 9,410 bridges in its inventory, 90 % of which are managed by the South Carolina Department of Transportation (SCDOT) [1]. Most of these bridges—roughly 75 %—are situated in rural regions. According to the SCDOT, 3,622 bridges were designed using either H-10 or H-15 loading criteria. The current design standard is called HL-93 and is significantly larger than the H-10 and H-15 loading criteria used in the 1950 s [2]. The average age of the bridges in South Carolina is 38.6 years, very close to the 50-year service life and 6.8 % of them are load-posted bridges. Weigh-in-motion (WIM) system are placed at 10 sites to restrict overweight vehicles from passing through these bridges. Moreover, with over 30 % of its bridges under-designed and suffering from decades of service deterioration, the SCDOT has made it a priority to evaluate these bridges and determine whether they need to be repaired or replaced.

Weigh-in-motion system consists of sensor and data analysis equipment. The system is employed to measure the weight of the vehicles in order to limit the number of overweight vehicles passing through the bridge without disrupting the flow of traffic [3]. Heavy, overweight vehicles cause overloading on the bridge, accelerating the wear of the road pavement and increasing the cost of repair [4,5]. Similarly, a large number of accidents are caused by overloaded vehicles due to their instability. Hence, WIM system is employed for cost optimization and to improve road safety.

Piezoelectric sensors, load cells, and bending plate sensors are the most commonly used commercially available WIM sensors [6,7]. But piezoelectric sensors are only suitable for the collection of traffic data and cannot be used to measure the weight, WIM systems with load cells

---

have large cross sections, and bending plate sensors are heavy and bulky. Moreover, the WIM sensors must be embedded in the pavement, which requires lane closure from several days to as long as a week. Therefore, it is necessary to investigate compact, lightweight, and reliable sensors to measure the load of the vehicles that can be quickly and readily placed in the field. This paper aims to explore the possibility of using acoustic emission (AE) system employing the AE sensors to determine vehicle loads while monitoring damages on the bridge.

With the development of sensor technology, various sensors have been used in structural health monitoring of structures [8,9]. Among them, AE sensors are popularly used because of their simplicity in application, high damage sensitivity, and ability to continuously monitor the response of civil infrastructures [10–14]. The application of AE sensors aids in automation and saves time and money on inspections without compromising the functionality of the structures [15,16].

In the AE system, AE sensors are used to collect AE data from the structures which are processed to obtain AE parameters such as amplitude, frequency, rise time, and AE energy. AE parameters are analyzed to evaluate the damage in the structure, including the detection of the cracks, location of the crack, type of the crack, and corrosion [17–20]. The performance of externally reinforced concrete beams was investigated using acoustic emission [21]. Average frequency (ratio of counts and duration) and rise time ratio (ratio of rise time and maximum amplitude) were used to differentiate the load at the crack initiation and characterize different damage mechanisms. Vandecruys et al. [22] investigated the progression of crack and location of corrosion damage in four RC beams using AE technique. AE events were analyzed which gave an indication of initiation of the crack and location of corrosion zone. Zhou et al. [23] performed static experiment on three different RC composite slabs. AE parameters: duration time, rise time, and energy, were used to analyze the characteristics of the damage, and the relation between the AE parameters and the load carrying capacity of the slab was investigated. The AE parameters were found to be directly proportional to the load resisting capacity of the RC slabs. Damage in the slabs were quantified using AE intensity analysis. Experiments were conducted on reinforced concrete (RC) beams, employing AE to classify shear and tensile cracks based on the statistical analysis of AE parameters; rise time ratio, and average frequency [24]. Elbatanouny et al. [25] investigated the monitoring abilities of AE on eight prestressed concrete *T*-beams subjected to cyclic load testing. Damages to the beams were quantified using amplitude and signal strength. Prem et al. [26] attached AE sensors to the damaged beams that were strengthened with ultra-high-performance concrete and tested them until failure. Through analytical monitoring of acoustic signals and acoustic emission interpretation of rise time ratio and average frequency, damage mechanisms were divided into five zones, and AE data was used to classify the type of the crack, shear or tensile, formed in the beams.

Even though a large number of AE parameters are collected, only a few of these parameters, such as amplitude, rise time, and AE energy, are used in statistical analysis for health monitoring of structures. When the analysis is based on a single parameter, loss of information is encountered due to the presence of noise data, resulting in a failure to provide an accurate evaluation of cracks and overall damage in the structure [27,28]. Multiple AE parameters should be simultaneously accounted to overcome the limitations of traditional analysis method [29]. Due to recent advances in data analysis methods, neural networks are commonly used to simultaneously interpret a large number of parameters in order to reach a strategic decision [30,31].

Artificial neural network (ANN) has been used to analyze AE data to carry out health monitoring of composite structures [32,33], railroads [34,35], and early warning systems in aeronautical engineering [36,37]. Selecting multiple AE parameters were found to increase the efficiency of the neural network significantly [38]. An indoor experiment was designed to investigate the relationship between eight AE signal parameters, loads, and cracks in prestressed beams [39]. A Deep Neural Network model was utilized to classify the structural damage. The findings were applied to two on-site bridges and the authors were able to detect certain problem areas based on the acoustic emission data. Source localization of impacts on an aircraft component into three zones was investigated by analyzing 15 features using an ANN [40]. Hassan et al. [41] reviewed the literature surrounding four different AI methods for the classification of AE data, including ANN, fuzzy logic, genetic algorithms, and support vector machines. ANN was found to be the most popular method due to its excellent ability to learn, extrapolate and recognize pattern to classify the input AE data effectively and efficiently. The powerful computational ability has increased the application of the ANN for monitoring the damage in structures [42]. However, there are limitations of using a single ANN, such as classifying datasets with random mistakes and networks with inadequate data for training. These can be eliminated by creating an ensemble ANN [43,44]. An ensemble ANN is a technique of combining multiple different ANN models into a classification algorithm to improve the performance of the ANN. Ensemble ANNs performed better at classification than the monolithic ANNs [45–49]. Li et al. [50] presented a method to identify defects and damage severity in a beam by comparing the frequency response functions of intact and damages structures using ANN. An ensemble ANN was implemented in the study to solve the issue of training convergence due to large data size. An ensemble ANN produced the most accurate result in predicting the location of defects and their severity in the experimental beam compared to the individual ANN.

The paper aims to explore the possibility of using small, lightweight, and easily applicable AE sensors in place of WIM systems to determine vehicle loads on bridges while simultaneously monitoring the bridge damage. The authors are currently not aware of any published work that uses AE to determine the vehicle loads. ANN has been implemented in the study to interpret a large number of AE parameters simultaneously to reach a strategic decision. Furthermore, an ensemble ANN is created to improve the performance of a single ANN and eliminate its inability to classify datasets with insufficient training data. The key contribution of this study is to create a load determination method using an ensemble ANN, to examine the AE data collected from the AE sensors to determine the vehicle loads in the bridges. The rest of the paper is organized as follows. Section 2 presents the experimental setup. Section 3 provides the information on analysis procedures. Section 4 is the results and discussion. The conclusions are summarized in Section 5.

2. Experimental setup

2.1. Test specimens

Flexural tests were conducted on two precast RC flat slabs provided by the SCDOT to simulate the vehicle loads passing over the bridge. The slabs were originally a portion of a bridge for a minimum of 30 years and later stored in an SCDOT facility. The slabs were 15 feet long, 8.25 in. thick and 5.5 feet wide (Fig. 1). Typical reinforcement details for the slabs consist of No. 7 bars at 6 in. on center longitudinally and No. 4 bars at 12 in. on center transversely (Fig. 2). The compressive strength of concrete and the yield strength of steel were 4,000 psi and 60,000 psi, respectively.

2.2. Test setup

Two 15-foot simply supported precast RC flat slabs were subjected to a four-point bending test [51] in the lab at the University of South Carolina (U of SC). To reduce friction at the supports during the application of the load, the slabs were placed on 9 in. bearing pads above the support. The clear span of the slab is 13.5 feet. The test numbering scheme, along with a brief description of the slabs, are presented in Table 1.

A hydraulic actuator was used to apply the load and a load cell was used to monitor the load values. A steel spreader beam was installed between the hydraulic actuator and the specimen at the mid-span of the
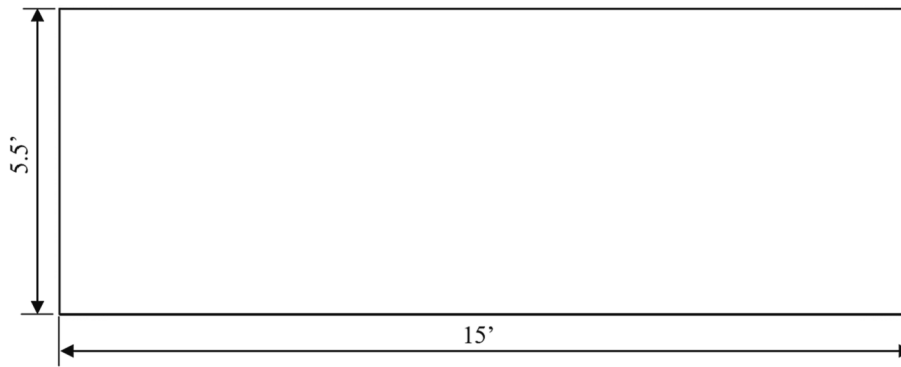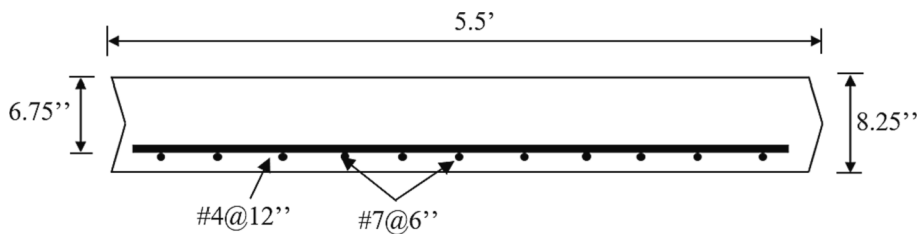
Fig. 1. Dimensions of the slabs.

Fig. 2. Reinforcement details of the slabs.

Table 1
Slab characteristics and geometry.

Test	Location of Test	Source of slabs	Date of Test	L (ft.)	W (ft.)	D (in.)
T1	U of SC	Calhoun Falls bridge	8/20/21	15	5.5	8.25
T2	U of SC	Calhoun Falls bridge	7/22/21	15	5.5	8.25

slabs (Fig. 3). A four-point bending arrangement was accomplished by adding neoprene pads between the hydraulic actuator and the steel spreader beam. The loading configuration replicates the AASHTO HL-93 design tandem with 4 feet of axle spacing [52], which produces the largest constant moment in the slabs. Photos of the test setups are presented in Fig. 4 and Fig. 5.

The loading on the slabs was stepwise cyclic. The slab was initially loaded to 2 kip. The load was increased to 10 kip, held there, and then unloaded back to 2 kip (referred to as load step 1, L1). Next, the load was increased to 20 kip, held there, and then unloaded back to 2 kip (referred to as load step 2, L2). The slab was then loaded to 30 kip, held there, and then unloaded back to 2 kip (referred to as load step 3, L3). The load versus time graph designed for the tests is illustrated in Fig. 6. The load steps 1 through 3 were designed in the study because it is the anticipated range of vehicle loads that these slab superstructures may support throughout their lifetimes.

2.2.1. Acoustic emission

AE is defined as the transient elastic waves within a material, caused by the rapid release of localized strain energy [53]. The recording of a particular signal is referred to as a "hit". The sensor response of a hit is in the form of a wave, which can be analyzed to obtain various parameters like amplitude, counts, duration, rise time, peak, and energy (Fig. 7). These parameters should cross a certain value to be captured, called a threshold, which is used to filter the noise signals during data collection.

Acoustic emission data was collected using the Sensor Highway II data acquisition system and four broadband sensors (type WDI). The sensors have an operating frequency range of 100–900 kHz. This wide range ensures that the sensor can effectively collect the slab response with different frequencies. An attenuation test has been conducted to
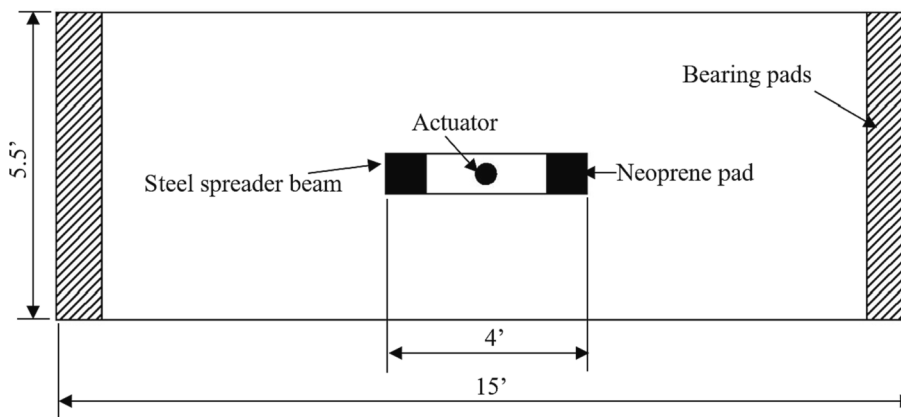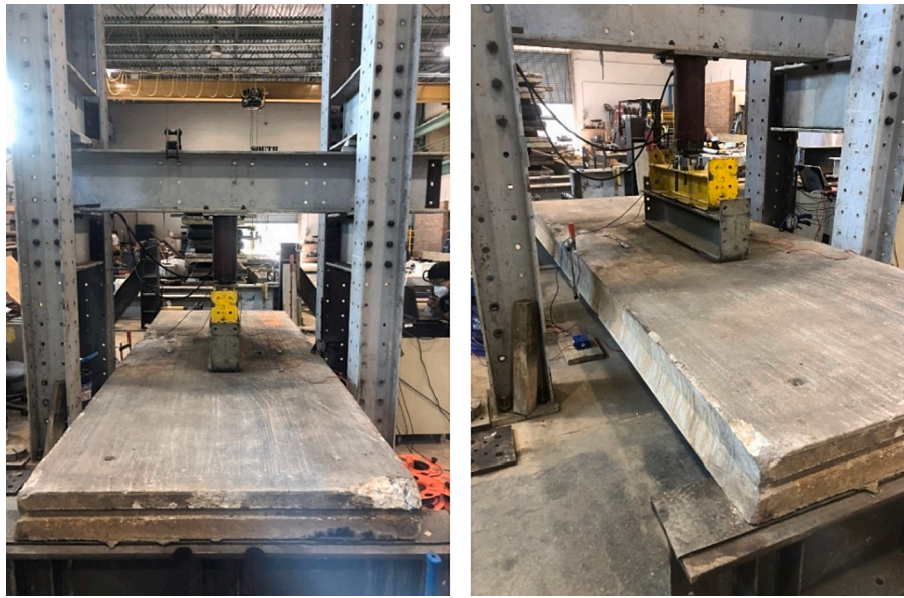

Fig. 3. Test setup of the slabs.

Fig. 4. Photos of the test setup T1.

Fig. 5. Photos of the test setup T2.

verify the sensitivity of WDI sensors by performing the Hsu-Nielsen pencil lead break. The results indicated that the sensors were sensitive to receive the signals from the farthest location on the specimen surface. The system was produced by the MISTRAS Group, Inc. of Princeton Junction, New Jersey. Broadband sensors were selected because they have a wider range of operating frequencies than the resonant AE sensors. The sensors were placed at a distance of L/3 and W/3 along the longitudinal and transverse direction respectively, as illustrated in Fig. 8. The sensors were attached to the specimen using double/bubble epoxy.

With a threshold of 50 dB (dB), data was continuously collected as the test progressed. The threshold was determined to prevent extraneous data from being picked up by the sensors. Peak definition time (PDT), defined as the interval between threshold crossing and peak amplitude, was set at 200 μs. The peak of a hit is found using this parameter. Hit Definition Time (HDT), which is set to 400 μs, is the time after which the

recording will be stopped. If hits with threshold crossings are not observed during HDT, hit recording will be stopped. A hit lockout time (HLT) of 800 μs is set to ensure any threshold crossing during this period will not be used in a hit waveform.

3. Analysis procedure

AE hits were collected during the flexural tests with the Sensor Highway II data acquisition system for further analysis. Single attribute analysis and an analysis using an ANN were implemented in the study to classify the AE hits to their corresponding vehicle loads based on their corresponding AE parameters.

3.1. Single attribute analysis

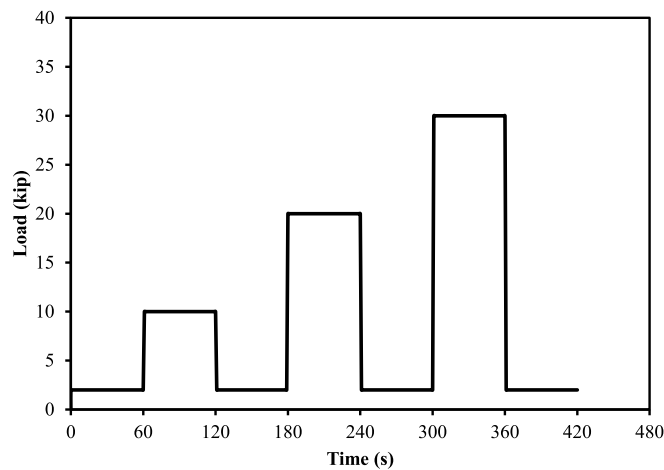The first attempt at classification analysis was performed to extract
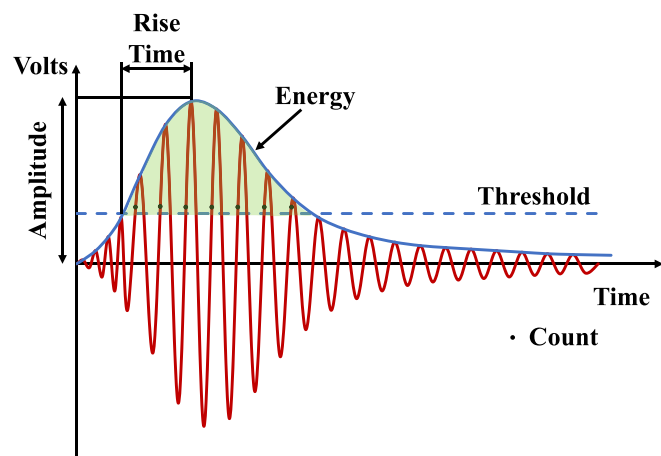
Fig. 6. Load vs Time.

Fig. 7. Definitions of AE parameters.

single attribute data from the test T1 and determine whether the attribute was a reliable indicator for the classification of the AE hits to their respective load steps. Due to the lack of consequential data collected from the AE hits in L1, the classification was done only on the AE hits belonging to the load steps L2 and L3. Three AE parameters, amplitude, rise time, and energy, were analyzed using basic statistical analysis to classify the AE hits to their corresponding load steps.

3.2. Artificial neural network

Artificial Neural Network (ANN) is a computing system inspired by biological neural networks [54,55]. It is composed of an input layer, a series of hidden layers, and an output layer. An ANN consisting of three layers: j, i, and k, is shown in Fig. 9, where j is an input layer, i is a hidden layer, and k is an output layer. Numerous processing units known as neurons are present in each layer, and each neuron is interconnected with others. The layer j has m, i has n, and k has l number of neurons. m represents the number of variables and l represents the number of outputs in the network. The number of neurons in the hidden layer, n, is selected to optimize the configuration of the network. Weights used to transform the data between the input, hidden and output layers are denoted by $W_{(ij)}$ and $W_{(kj)}$.

Due to the large number of data points collected during the test and the large number of features related to these AE hits, an artificial neural network was developed to classify the AE hits into two load steps: L2 and L3. Table 2 lists the 13 AE parameters and their definitions that were used in the study. The neural network goes through three steps for the classification AE hits: training, validation, and testing.

Data from T1, which included the AE hits, about 23,000 hits from T1L2 (data collected during test 1 and load step 2) and T1L3 (data collected during test 1 and load step 3), was fed into the neural network. It randomly selected one-third of the data for training, another third for validation, and the final third for testing. The majority of the data in the total data set belonged to T1L3, which led to an imbalance issue in the network. The network became particularly good at classifying the data from T1L3 but was inaccurate at classifying the data from T1L2. Fig. 10 shows the initial process of the neural network.

To address the imbalance issue, an improved ANN was developed that would train, validate, and test an equal number of data from each load step. It was determined that the number of data belonging to T1L3 was about ten times that of T1L2. To even out the data, ten different models were trained and validated with all the data from T1L2 and a random tenth of the data from T1L3. This process is referred to as "balanced training". These models were then tested on the data that was taken before training or validation, and each model cast a classification vote. The majority rule applied to the votes of the model, and a final classification was determined, thus creating an improved ensemble ANN. Fig. 11 shows the process of the neural network ensemble.

Once the algorithm was established, the optimal number of hidden layers as well as the optimal hidden layer size were determined through trial-and-error method. The optimal number and size were determined based on the output accuracy. Once optimized, this model was named MT1 (the model trained on the data from the test T1).

After the algorithm was optimized, robustness of the trained neural network was tested on the data collected from an entirely different slab
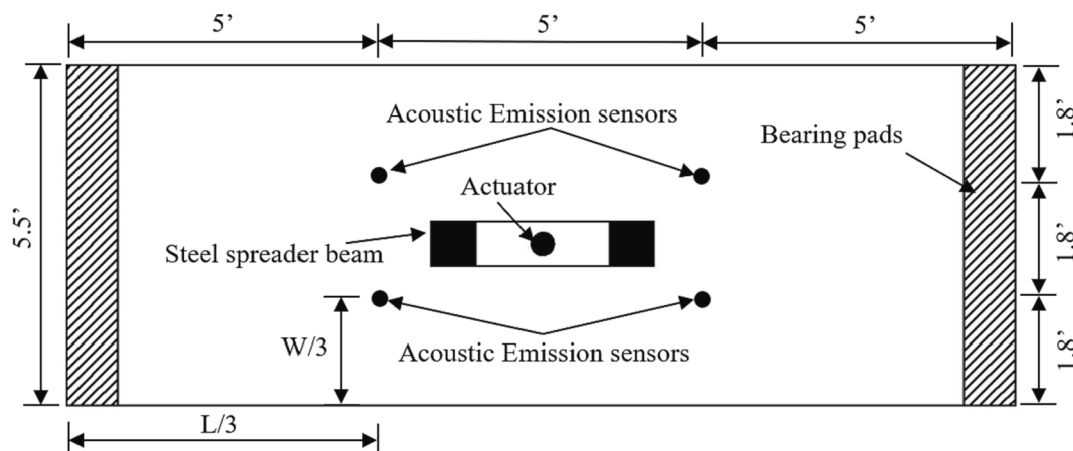

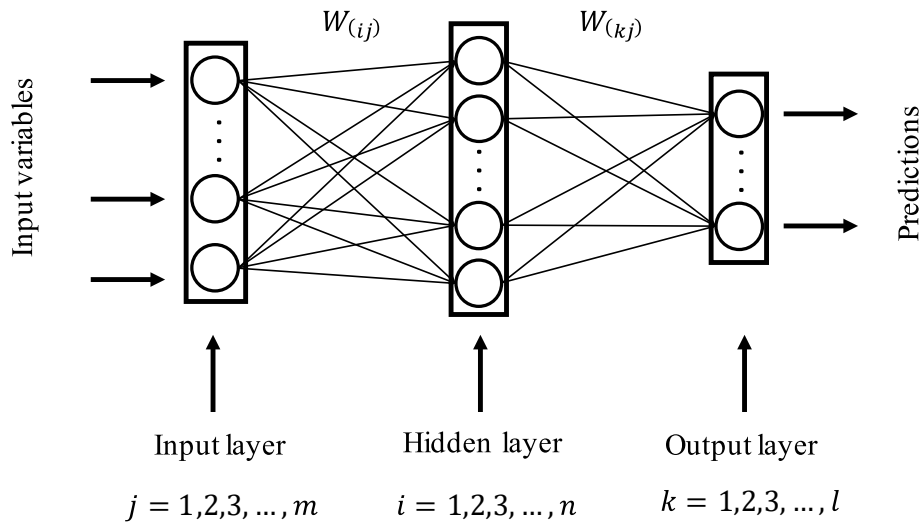**Fig. 8.** A scheme of the test setup and AE sensor locations.

Fig. 9. Structure of a 3-layer ANN.

Table 2
AE parameters and definitions.

Number	AE parameters	Descriptions
1	Amplitude (dB)	The maximum amplitude at the peak
2	Count	The number of threshold crossings
3	Rise time (μs)	Time interval between first threshold crossing and maximum amplitude
4	Duration (μs)	Time between first and last threshold crossing of signal
5	Average frequency (kHz)	Counts/Duration
6	Root mean square (RMS) (V)	The effective voltage with a characteristic time T_{RMS} for average ranging from 10 to 1000 ms
7	Average signal level (ASL) (V)	The effective voltage with a characteristic time T_{ASL} for average ranging from 10 to 1000 ms
8	Energy (10^{-14} V^2s)	The measure of the electrical energy measured for an AE signal
9	Absolute energy	The absolute measure of the electrical energy measured for an AE signal
10	Reverberation frequency (kHz)	Frequency after the peak
11	Initial frequency (kHz)	Frequency before the peak
12	Signal strength	A parameter to evaluate the AE source strength
13	Counts to peak (PCNTS)	The number of threshold crossings from the first threshold crossing to the peak

Fig. 10. Initial flowchart for the ANN.

test. The neural network was trained using the data collected from T1, and the performance of the network was determined by the accuracy of the classification of the data collected from the test 2, T2. The classification ability of MT1 was determined by analyzing the accuracy in classifying the data belonging to T2L2 (data collected during test 2 and load step 2) and T2L3 (data collected during test 2 and load step 3). A flowchart of this process can be seen in Fig. 12.

4. Results and discussion

The stepwise cyclic loads were applied to the slabs during the flexural tests. AE hits collected from the tests were analyzed. This section shows the results obtained from the single attribute analysis and an analysis using ANN in classifying the AE hits to their corresponding load steps representing the vehicle loads on the slabs.

4.1. Single attribute analysis results

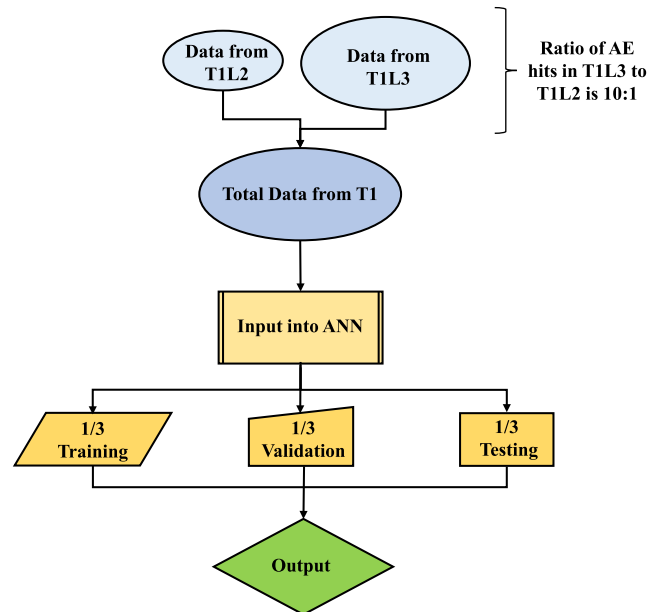The AE parameters such as amplitude, rise time, and energy can represent the main information of an acoustic emission signal and they were the most used parameters for structural health monitoring in the literature. Therefore, this section presents a single attribute analysis includes a statistical analysis of the AE parameters: amplitude, rise time, and energy of the AE hits, collected from the test T1.

4.1.1. Amplitude analysis

Amplitude was the first attribute analyzed. The amplitude of AE hits was plotted along with the loading and time of the test T1 (Fig. 13). It was determined that the AE hits from T1L1 would be insignificant due to the lack of consequential data collected during this step. Attention was then turned to the differences between T1L2 and T1L3. The plot showing the amplitudes in T1L2 and T1L3 look similar with a greater density of AE hits and a higher peak amplitude in T1L3 compared to T1L2.

To find more specific differences, simple statistics were extracted for T1L2 and T1L3. This data can be seen in Table 3, where the upper and lower limits were determined from the following equations, Eq. (1) and Eq. (2) respectively.

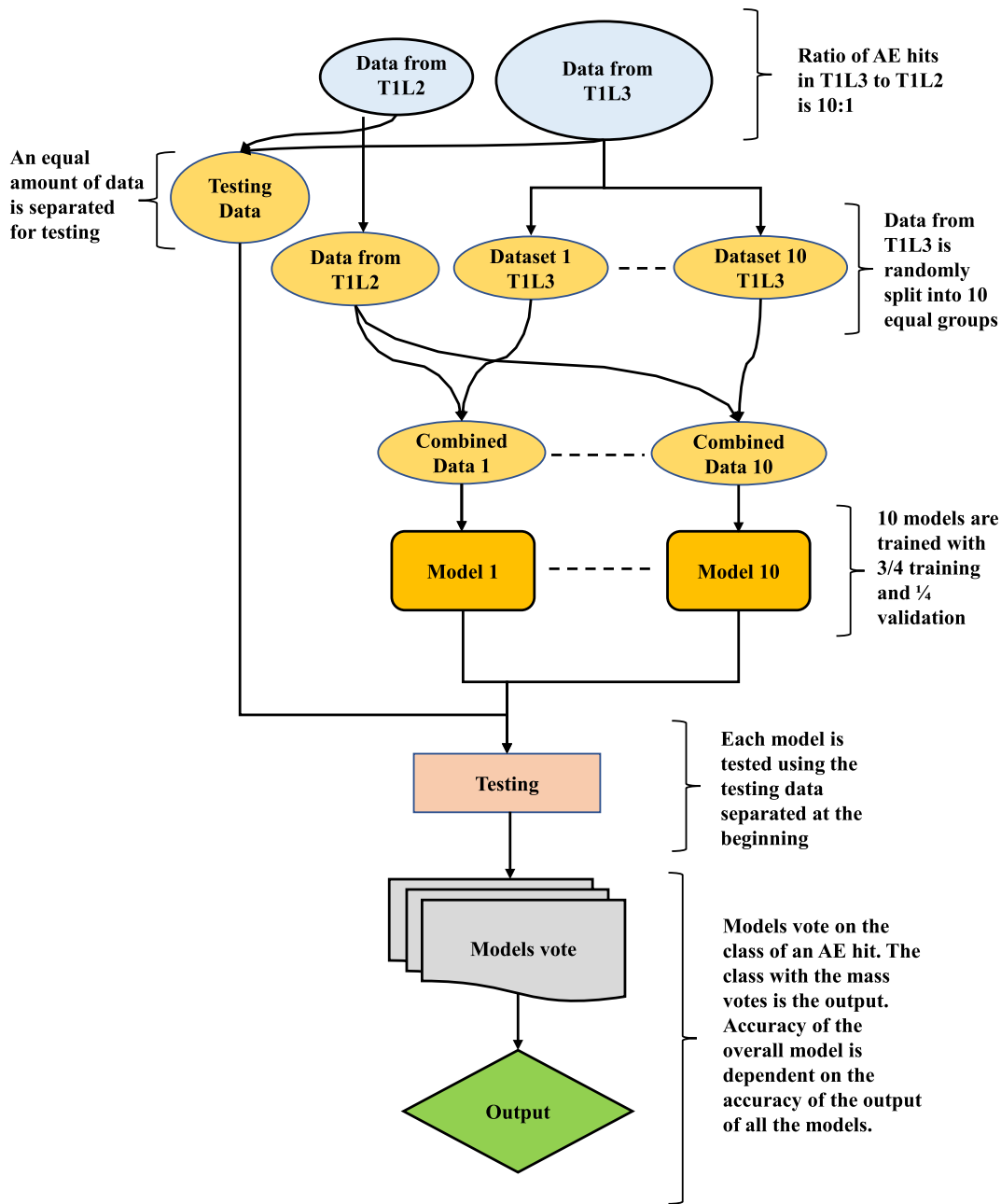$$\text{Upper Limit} = \mu + 3*\sigma \tag{1}$$

Fig. 11. Balanced training flowchart for the ANN.

$$\text{Lower Limit} = \mu - 3*\sigma \tag{2}$$

where μ is the mean and σ is the standard deviation of the sample.

The average amplitude of T1L2 was 56.4 dB and T1L3 was 57.3 dB. The standard deviation for T1L2 and T1L3 was 6.31 dB and 6.93 dB, respectively. The upper and lower limits for T1L2 were 75.3 dB and 37.4 dB, while the limits for T2L3 were 78.1 dB and 36.5 dB. The maximum amplitude achieved for T1L2 was 88 dB, while T1L3 reached a max amplitude of 99 dB. The number of AE hits collected during T1L2 was 2,263, and for T1L3 it was 20,981. The results obtained from the statistical analysis of amplitude parameter looks similar for T1L2 and T1L3, making it difficult to classify the AE hits to their respective load steps L2 and L3.

A probability chart was created by plotting the probability of an amplitude occurring within that load step. The probability is obtained by taking the number of AE hits of that amplitude and dividing it by the total number of AE hits in that load (Eq. (3)). This chart can be seen in

Fig. 14, which shows a similar pattern of probability of occurrence for the amplitudes in T1L2 and T1L3. Since, a significant difference in the probability chart cannot be found, the amplitude parameter may not be conclusive in the classification of AE hits to the load steps L2 and L3.

$$P_{A(L2)}(50) = \frac{\text{Number of 50 amplitude AE hits in T1L2}}{\text{Total number of AE hits in T1L2}} \tag{3}$$

4.1.2. Rise time analysis

After comparing the amplitude, the rise time of AE hits was plotted along with the loading and time of the test T1 Fig. 15. For rise time analysis also, AE hits from T1L1 would be insignificant due to the lack of consequential data collected during this step. The plot showing the rise time in T1L2 and T1L3 look similar with a greater density of AE hits and a higher peak rise time in T1L3 compared to T1L2.

The rise time was then statistically analyzed, and the statistical data are shown in Table 4. The average rise time of T1L2 was 82.3 μs and
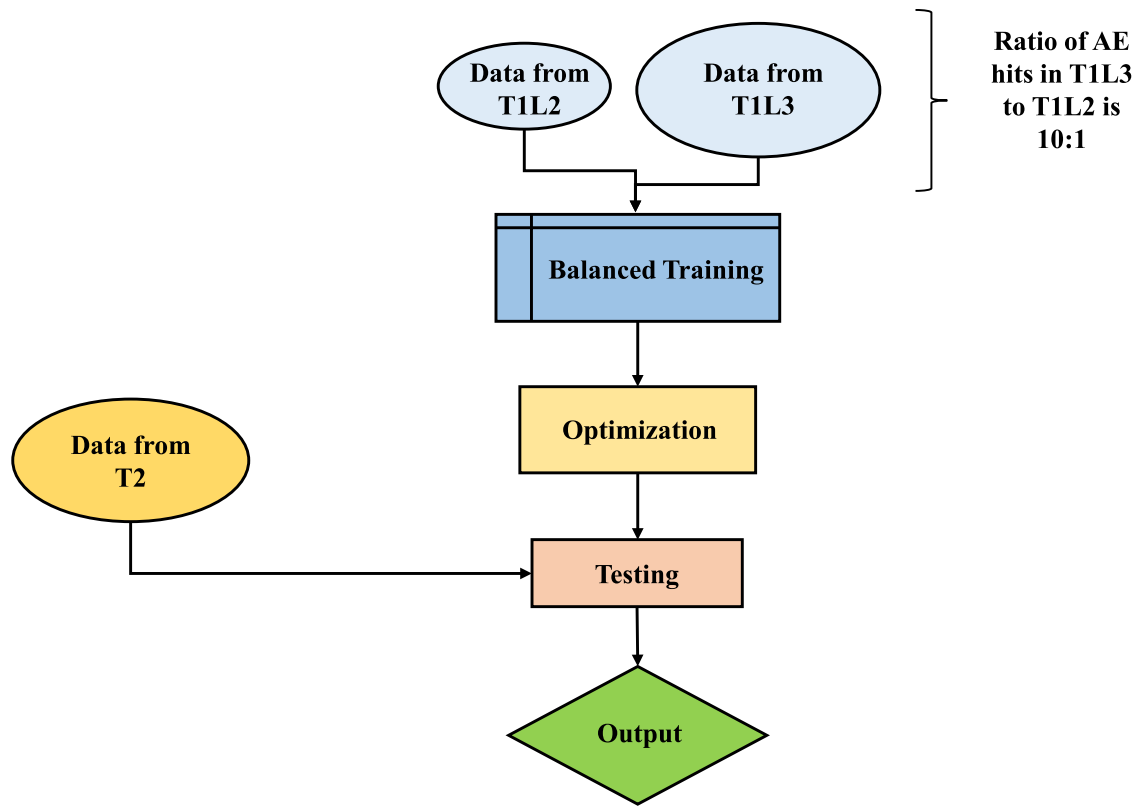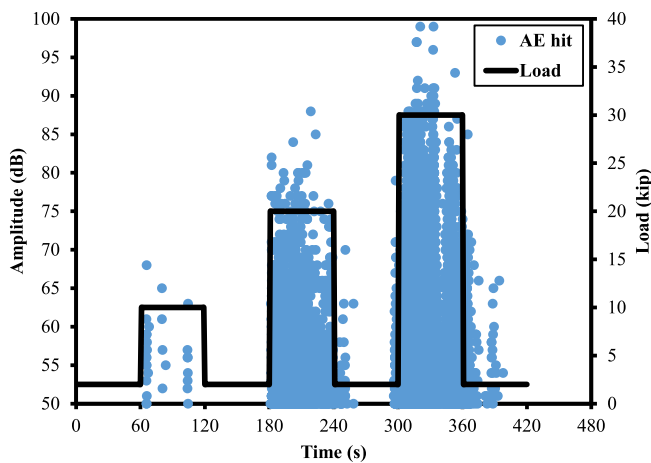
Fig. 12. Robustness of MT1 model.
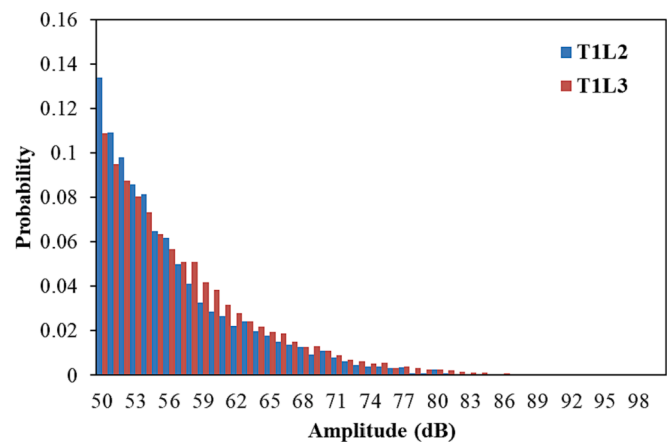

Fig. 13. Load & Amplitude vs time for T1.

Fig. 14. Amplitude probabilities for T1L2 & T1L3.

rise time achieved for T1L2 was 661 μ*s* while T1L3 reached a maximum rise time of 1430 μ*s*. The differences in the basic statistics in the rise time were more apparent than the amplitude parameter. However, there are AE hits in T1L2 and T1L3, which have the same rise time. The rise time for the AE hits in T1L2 ranges from 0 μ*s* to 661 μ*s* and the AE hits in T1L3 ranges from 0 μ*s* to 1431 μ*s*. The range of the AE hits in T1L2 lies within the range of the AE hits in T1L3 until 661 μ*s*. As a result, based on the rise time, it is difficult to classify these AE hits to their respective load steps L2 and L3.

The probability of each rise time was plotted according to Eq. (4) to find out if it is possible to use rise time for the classification of the AE hits (Fig. 16). It is challenging to utilize these plots for rise time to differentiate the AE hits to their respective load steps L2 and L3, since they do not demonstrate any notable distinctions.

Table 3
Amplitude statistics for T1.

Amplitude (dB)	T1L2	T1L3
Mean	56.4	57.3
Standard deviation	6.31	6.93
Upper limit	75.3	78.1
Lower limit	37.4	36.5
Upper range	88	99
Lower range	50	50
Number of AE hits	2263	20,981

T1L3 was 123 μ*s*. The standard deviation for T1L2 and L3 was 89.1 μ*s* and 154 μ*s*, respectively. The upper and lower limits for T1L2 were 350 μ*s* and 1 μ*s* while the limits for T1L3 were 586 μ*s* and 1 μ*s*. The maximum

Fig. 15. Load & Rise time vs time for T1.

Table 4
Rise time statistics for T1.

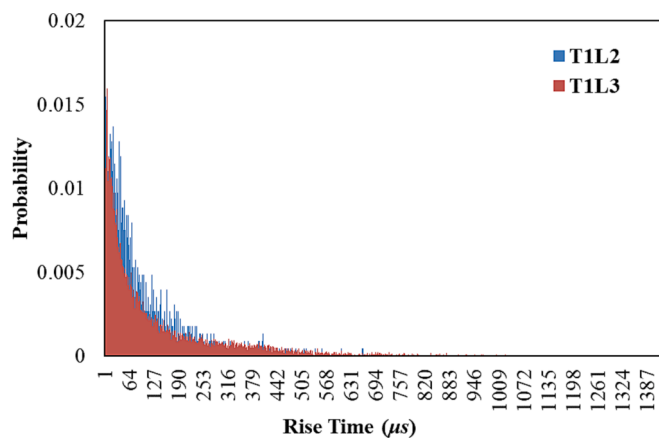| Rise time (µs)	T1L2	T1L3
Mean	82.3	123
Standard dev	89.1	154
Upper limit	350	586
Lower limit	0	0
Upper range	661	1430
Lower range	1	1
Number of AE hits	2263	20,981

Fig. 16. Rise time probabilities for T1L2 & T1L3.

$$P_{R(L2)}(52) = \frac{\text{Number of AE hits with rise time } 52\mu s \text{ in T1L2}}{\text{Total number of AE hits in T1L2}} \quad (4)$$

4.1.3. Energy analysis

Lastly, the energy of AE hits was plotted along with the loading and time of the test T1 Fig. 17. For the energy also, AE hits from T1L1 would

be insignificant due to the lack of consequential data collected during this step. The plot showing the rise time in T1L2 and T1L3 look similar with a greater density of AE hits and a higher peak energy in T1L3 compared to T1L2.

The energy parameter was statistically analyzed, and the results are presented in Table 5. The average energy of T1L2 was $12.2 \times 10^{-14}V^2s$ and T1L3 was $21.9 \times 10^{-14}V^2s$. The standard deviation for T1L2 and T1L3 was $20.8 \times 10^{-14}V^2s$ and $56.5 \times 10^{-14}V^2s$, respectively. The upper and lower limits for T1L2 were $74.5 \times 10^{-14}V^2s$ and $0 \times 10^{-14}V^2s$ while the limits for T1L3 were $191 \times 10^{-14}V^2s$ and $0 \times 10^{-14}V^2s$. The maximum energy achieved for T1L2 was $349 \times 10^{-14}V^2s$, while T1L3 reached a maximum energy of $1920 \times 10^{-14}V^2s$. The differences in the basic statistics for energy were less apparent than the rise time parameter but more apparent than the amplitude parameter. The energy parameter also suffers from the same problem as the rise time where the AE hits in T1L2 and T1L3 have same energy since the range of energy of the AE hits for T1L2 from $0 \times 10^{-14}V^2s$ to $349 \times 10^{-14}V^2s$ lies within the range of $0 \times 10^{-14}V^2s$ to $1920 \times 10^{-14}V^2s$ of T1L3. It is therefore difficult to classify
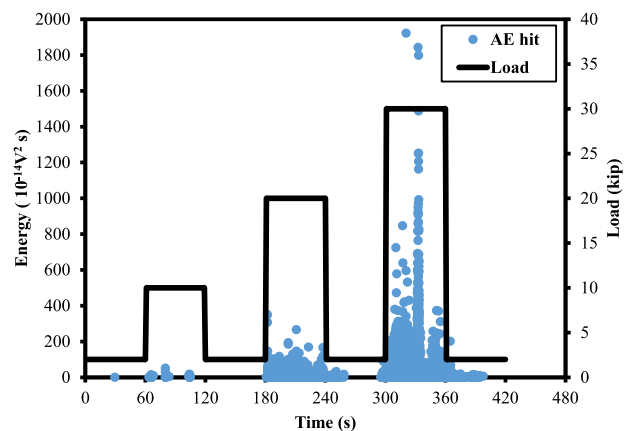

Fig. 17. Load & Energy vs time for T1.

Table 5
Energy statistics for T1.

Energy (10^{-14}V^2s)	T1L2	T1L3
Mean	12.2	21.9
Standard deviation	20.8	56.5
Upper limit	74.5	191
Lower limit	0	0
Upper range	349	1920
Lower range	0	0
Number of AE hits	2263	20,981

these AE hits to their load steps L2 and L3 based on the energy.

The probability of the energy was plotted using Eq. (5) to find out if it is possible to use energy for the classification of the AE hits (Fig. 18). The plots for the probability of AE hits with the energy level for T1L2 and T1L3 are similar. Therefore, it is difficult to use the data for the classification the AE hits to their respective load steps L2 and L3.

$$P_{E(L2)}(14) = \frac{\text{Number of AE hits with energy 12 in T1L2}}{\text{Total number of AE hits in T1L2}} \quad (5)$$

In this section, statistical analysis of three AE parameters is presented. The goals of this analysis were to a) quantify the differences between the AE parameters collected during different load steps and b) determine whether the differences can be exploited to classify the data. It was concluded that, while there are some statistical differences, it is difficult to classify the AE hits from a single attribute analysis to their corresponding load steps L2 and L3. This conclusion led to the construction of an ANN that allowed analysis of 13 attributes for classification of the AE hits into the respective load steps L2 and L3.

4.2. ANN results

An artificial neural network was developed to classify the AE hits using 13 parameters extracted from the Sensor Highway II system. The goal of the algorithm was to accurately classify AE hits into their corresponding load steps. The performance of the model was measured in terms of recall: ratio of the number of correctly classified AE hits in a load step over the total number of AE hits in the load step, and accuracy: ratio of the number of correctly classified AE hits over the total number of AE hits for that test. The precision, ratio of the number of correctly classified AE hits in the load step over the total number of AE hits pre-

dicted in the load step, measured by the model is not of significant importance due to the large amounts of data present in each load step. Some of the AE hits predicted wrongly will not have a negative impact on the overall prediction. The recall, accuracy, and precision are calculated using Eq. (6), Eq. (7), and Eq. (8), respectively.

$$\text{Recall} = \frac{\text{Number of correctly classified AE hits in the load step}}{\text{Total number of AE hits in the load step}} \quad (6)$$

$$\text{Accuracy} = \frac{\text{Number of correctly classified AE hits in the test}}{\text{Total number of AE hits in the test}} \quad (7)$$

$$\text{Precision} = \frac{\text{Number of correctly classified AE hits in the load step}}{\text{Total number of AE hits predicted as the load step}} \quad (8)$$

4.2.1. Performance of the original ANN

The first neural network took data from T1, which included all the AE hits from T1L2 and T1L3 (over 23,000). AE hits, with their corresponding parameters, were labeled as L2 and L3. The neural network received these datasets as input. The neural network randomly selected one third of the data for training, another third for validation, and the last third for testing. The neural network classified the AE hits based on the 13 parameters to load steps L2 and L3.

The confusion matrix of the test is shown in Fig. 19. The numbers of AE data that are correctly localized in their corresponding classes are shown in the main diagonal of the confusion matrix. Out of 2,263 AE hits recorded in L2, 570 AE hits were correctly classified to L2 while 1,693 AE hits were incorrectly classified to L3. Out of the 20,981 AE hits in L3, 20,545 were correctly labeled as L3 and 436 were incorrectly classified to L2. In total, 21,115 AE hits out of 23,244 AE hits were correctly classified into their corresponding load steps, meaning the overall accuracy is 90.8 %. In addition to accuracy, precision, and recall for each class are usually implemented to evaluate the performance of classification in each class. The ANN model had a 25.2 % recall rate in the classification of L2, a 97.9 % recall rate in the classification of T1L3, The model is accurate at classifying L3; however, it is inaccurate in the classification of L2, causing an imbalance issue (the model is accurate at classifying L3; however, it is inaccurate in the classification of L2). This issue occurred because the model takes a random third of the data set for training, validation, and testing. The problem with this method is that the number of AE hits in the dataset belonging to T1L3 outnumbered the AE hits belonging to T1L2 by a ratio of 10:1.
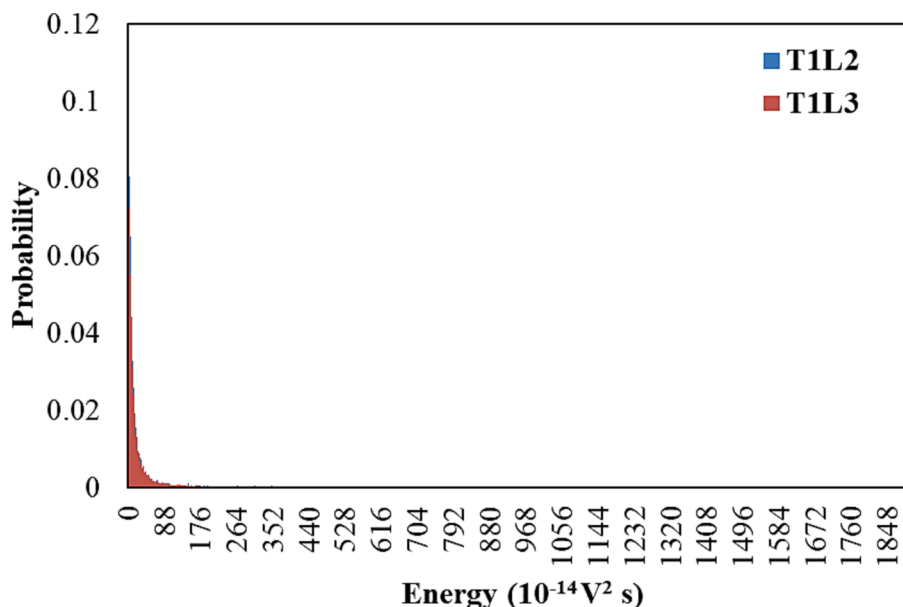

Fig. 18. Energy probabilities for T1L2 & T1L3.

Recall

Fig. 19. Confusion matrix of imbalanced training on Test T1.

4.2.2. Performance of the improved ensemble ANN

To address this issue of imbalance, a balanced training and testing data set was developed where 10 different models were trained using even data from both T1L2 and T1L3. Moreover, the models were tested, each model voted, and the classification of the load step was determined by the majority of the models. This improved ensemble ANN had a 90.5 % recall rate in the classification of T1L2; 410 AE hits out of 453 AE hits were correctly assigned to L2, whereas 43 AE hits were incorrectly classified to L3. It had an 81.2 % recall rate in the classification of T1L3; out of 421 AE hits, 342 AE hits were accurately assigned to L3, whereas 79 AE hits were incorrectly classified to L2. An overall accuracy of 86.0 % was attained in the model. The overall accuracy of the model has dropped by 4.8 %, but the recall rate of T1L2 increased by 65.3 % due to the balance in the training data for both T1L2 and T1L3. This model is much better suited to classifying both T1L2 and T1L3 AE hits. The confusion matrix for this model can be seen in Fig. 20.

4.2.3. Optimization of ANN

The improved ensemble ANN model was further optimized by determining the ideal number of neurons and hidden layers for a more

Fig. 20. Confusion matrix of balanced training on Test T1.

balanced performance in classifying the AE hits. The model was run 10 times for every neuron size from 20 to 30, and an average overall accuracy was determined. An average was taken because the selection of data is random, which lead to a slight variability in performance from test to test. An optimal neuron number was found. The same process was repeated for the hidden layer size. The optimal number of neurons was found to be 23, and the ideal hidden layer size was determined to be one with the overall accuracy of the model being 85.65 %. Accuracies for models with varying neuron numbers and varying numbers of hidden layers can be found in Table 6 and Table 7.

4.2.4. Robustness of the ANN

Once optimized, this model was named MT1, and then tested against the 7,641 AE hits recorded in the test T2 to observe its reliability against the data that it had never seen before. The AE hits were classified to load steps L2 and L3, and the result of the model is shown in the confusion matrix shown in Fig. 21. Out of 756 AE hits in T2L2, 702 were correctly labeled to L2 while 54 were incorrectly classified to L3. Out of 6,885 AE hits, 4,874 AE hits were correctly assigned to L3 while 2,011 AE hits were incorrectly classified to L2. The model, which was trained solely on the T1 dataset, had a recall rate of 92.9 % in classifying AE hits in T2L2 and a recall rate of 70.8 % in classifying AE hits in T2L3, with an overall accuracy of 73.0 %. The classification test using T2 data, showed the ability of the ANN model to classify unfamiliar data with an error of 27 %. This is a preliminary study, so the accuracy of a well performing model has yet to be set.

In this section, an algorithm was developed that utilized an artificial neural network to classify the AE hits to their corresponding loads using the differences of all 13 parameters instead of single parameter only. The idea prompting this method being that the small variances of the 13 parameters would allow the system to accurately classify the data points.

The initial analysis showed the need for a balanced training method in order to accurately classify both load steps. The improved ensemble ANN created after the balanced training showed the ability to overcome the imbalance of testing data and to accurately classify the AE hits based on the 13 parameters. The model was able to classify the AE hits corresponding to the vehicle loads, 20 kip and 30 kip representing the design tandem with 4 feet of axle spacing, with an overall classification accuracy of 86.0 %.

Optimization of a neural network was done through an iterative process that resulted in a more balanced performance of the ANN. The classification test using T2 data showed the ability of the optimized improved ensemble ANN model to accurately classify the unfamiliar data. It also showed the ability for an ensemble ANN to classify the AE hits corresponding to the vehicle loads, 20 kip and 30 kip representing the design tandem with 4 feet of axle spacing, from an entirely different test with an overall accuracy of 73.0 %.

Hence, using the AE hits, the optimized improved ensemble ANN model developed in the study can be used to measure the 20 kip and 30 kip loads of the design tandem placed above the slab with a maximum error of 27 %.

5. Conclusion and recommendations

In this study, AE data was collected from flexural tests of two 15-foot precast RC flat slabs. Approximately 30,000 AE hits were analyzed and classified using statistical analysis of a single attribute of the AE hits. The paper then explored the possibility of using an improved ensemble ANN to classify AE hits into the load steps based on their 13 parameters. Following are the findings of the study:

1. The traditional method of statistical analysis based on single attributes of AE hits is not effective in classifying the AE hits to their corresponding vehicle loads.

Table 6
Optimization of neuron number.

Number of neurons	Accuracy %										Average %
20	84.6	86.3	84.2	86.4	86.8	84.4	85.8	84.6	83.8	86.2	85.31
21	83	84.7	82.6	83.4	85	84.2	85.1	87.9	83.5	85.1	84.45
22	84.2	84.8	85.1	84.4	87.8	85	84.4	85.7	84.9	85.2	85.15
23	84.9	86.2	85.7	85.1	87.2	87.6	83.2	84.4	85.9	86.3	85.65
24	86.7	85.2	85.6	84.4	84.6	84.8	83.8	86.6	83.2	85.7	85.06
25	85.4	85	84	86.5	86	85.6	87.1	86.6	85.5	85.1	85.68
26	84.7	86.5	84.4	83.8	84.6	84	85.6	84.7	84	84	84.63
27	84.3	86	86	87.4	85.8	85.6	85.1	84	85.5	84	85.37
28	85.2	84.4	85.7	86.3	87.1	84.1	86.7	85.5	84.7	84.2	85.39
29	87.1	85.7	83	85.1	84.6	86.4	86.3	83.5	84.9	87	85.36
30	87.1	84.4	83.5	84.9	85.4	83.5	85.2	84.6	84.9	86.3	84.98

Table 7
Optimization of number of hidden layers.

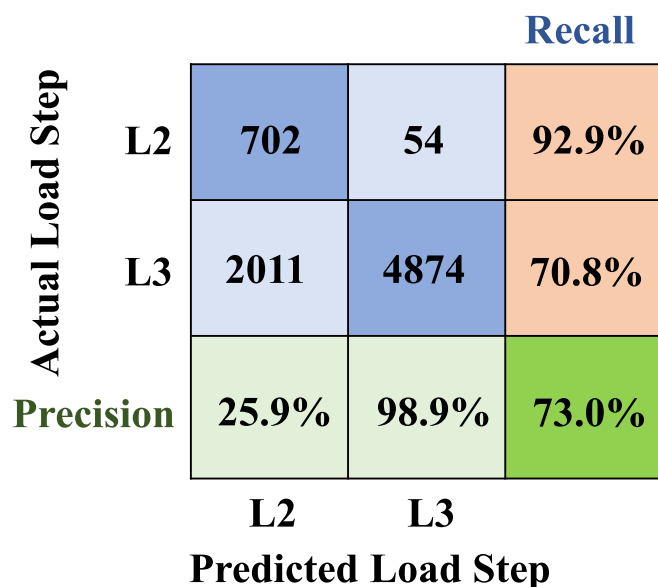| Hidden layers	Accuracy %										Average %
1	84.9	86.2	85.7	85.1	87.2	87.6	83.2	84.4	85.9	86.3	85.65
2	84.3	84.6	85	84.8	86.2	85.7	86.8	85.8	84.9	86.4	85.45
3	84.1	87	85.5	86.5	85.1	84.7	83.9	87.5	84.2	83	85.15

Fig. 21. Confusion matrix of MT1 tested on T2 data.

2. A single ANN experienced an imbalance issue because of insufficient training data where the ANN had a 25.2 % recall rate in the classification of T1L2 whereas a 97.9 % recall rate in the classification of T1L3.

3. Improved ensemble ANN overcame the imbalance issue in the testing data and improved the accuracy in classifying the AE hits belonging to T1L2. The ensemble ANN had an improved recall rate of 90.5 % in the classification of T1L2 and a recall rate of 81.2 % in the classification of T1L3.

4. The optimized improved ensemble ANN model was reliable in classifying the AE hits collected from the separate test, T2, with a recall rate of 92.9 % in classifying AE hits to T2L2 and a recall rate of 70.8 % in classifying AE hits to T2L3, with an overall accuracy of 73.0 %. Hence, AE in conjunction with an optimized improved ensemble ANN can be used to determine the vehicle loads in the slab.

More studies are needed to prove that the optimized improved ensemble ANN is a viable method for the classification of AE data.

Studies must be done with more load steps and smaller step sizes to predict the vehicle load based on the AE data collected. Studies must be conducted on other typical structures. AE is dependent upon the mechanical properties of the surface the transducers are attached to. The current study and neural network developed would only work for 15-foot precast RC flat slabs. Furthermore, the study only takes into account the application of a concentrated load on the slab, whereas vehicle loads in the real world are always dynamic. Therefore, studies should be conducted to gather the AE response from the dynamic vehicle loads on the slab, and an ensemble ANN should be employed to predict the dynamic loads on the slab.

Having access to enough AE data for the existing bridge is one of the practical issues for training a supervised learning method. Future research could focus on either the novel AE data augmentation method or utilizing numerical models to generate a large number of training data.

CRediT authorship contribution statement

Declaration of Competing Interest

The authors declare that they have no known competing financial interests or personal relationships that could have appeared to influence the work reported in this paper.

Data availability

Data will be made available on request.

Acknowledgments

References

[1] S. Carolina, The American Society of Civil Engineers, Sci. Am. 12 (1881) 4592–4593, https://doi.org/10.1038/scientificamerican07091881-4592bsupp.

[2] Aashto, AASHTO LRFD Bridge Design Specifications, 2020.

[3] B. Jacob, H. van Loo, Weigh-in-motion for enforcement in Europe, International Conference on Heavy Vehicles HVParis 2013 (2008) 25–38, https://doi.org/10.1002/9781118623305.ch1.

[4] R. Hou, S. Jeong, J.P. Lynch, M.M. Ettouney, K.H. Law, Data-driven analytical load rating method of bridges using integrated bridge structural response and weigh-in-motion truck data, Mech. Syst. Sig. Process. 163 (2022) 108128.

[5] M. Sujon, F. Dai, Application of weigh-in-motion technologies for pavement and bridge response monitoring: State-of-the-art review, Autom. Constr. 130 (2021) 103844.

[6] A.I. Dontu, P.D. Barsanescu, L. Andrusca, N.A. Danila, Weigh-in-motion sensors and traffic monitoring systems - Sate of the art and development trends, IOP Conf Ser Mater Sci Eng. 997 (1) (2020) 012113.

[7] T. Haugen, J.R. Levy, E. Aakre, M.E.P. Tello, Weigh-in-Motion Equipment - Experiences and Challenges, Transp. Res. Procedia 14 (2016) 1423–1432.

[8] X. Tan, Y. Bao, Q. Zhang, H. Nassif, G. Chen, Strain transfer effect in distributed fiber optic sensors under an arbitrary field, Autom. Constr. 124 (2021), 103597, https://doi.org/10.1016/J.AUTCON.2021.103597.

[9] J. Zhu, H. Sun, C. Malone, L. Ai, M. Bayat, P. Ziehl, T. Shin, Y. Zhang, E. Giannini, Online Monitoring System for Concrete Structures Affected by Alkali-Silica Reaction No. DOE-UNL-NE8544 (2021), https://doi.org/10.2172/1838356.

[10] C.U. Grosse, M. Ohtsu, Acoustic emission testing: Basics for Research-Applications in Civil, Engineering (2008), https://doi.org/10.1007/978-3-540-69972-9.

[11] P.H. Ziehl, Applications of acoustic emission evaluation for civil infrastructure, in: Nondestructive Characterization for Composite Materials, Aerospace Engineering, Civil Infrastructure, and Homeland Security 2008, 2008. https://doi.org/10.1117/12.779069.

[12] S. Patil, B. Karkare, S. Goyal, Corrosion induced damage detection of in-service RC slabs using acoustic emission technique, Constr. Build. Mater. 156 (2017) 123–130, https://doi.org/10.1016/j.conbuildmat.2017.08.177.

[13] N.B. Burud, J.M.C. Kishen, Response based damage assessment using acoustic emission energy for plain concrete, Constr. Build. Mater. 269 (2021) 121241.

[14] F. Liu, R. Guo, X. Lin, X. Zhang, S. Huang, F. Yang, X. Cheng, Monitoring the damage evolution of reinforced concrete during tunnel boring machine hoisting by acoustic emission, Constr. Build. Mater. 327 (2022) 127000.

[15] C.R. Farrar, K. Worden, An introduction to structural health monitoring, Philos. Trans. R. Soc. A Math. Phys. Eng. Sci. 365 (2007) 303–315, https://doi.org/10.1098/rsta.2006.1928.

[16] A. Entezami, Structural Health Statistical Distance Series Analysis and Monitoring by Time Measures, 2021.

[17] M. Di Benedetti, A. Nanni, Acoustic Emission Intensity Analysis for In Situ Evaluation of Reinforced Concrete Slabs, J. Mater. Civ. Eng. 26 (1) (2014) 6–13.

[18] H. Zeng, J.A. Hartell, M. Soliman, Damage evaluation of prestressed beams under cyclic loading based on acoustic emission monitoring, Constr. Build. Mater. 255 (2020), 119235, https://doi.org/10.1016/j.conbuildmat.2020.119235.

[19] R. Worley, M.M. Dewoolkar, T. Xia, R. Farrell, D. Orfeo, D. Burns, D.R. Huston, Acoustic Emission Sensing for Crack Monitoring in Prefabricated and Prestressed Reinforced Concrete Bridge Girders, J. Bridg. Eng. 24 (2019) 1–12, https://doi.org/10.1061/(asce)be.1943-5592.0001377.

[20] X. Tan, L. Fan, Y. Huang, Y. Bao, Detection, visualization, quantification, and warning of pipe corrosion using distributed fiber optic sensors, Autom. Constr. 132 (2021), 103953, https://doi.org/10.1016/J.AUTCON.2021.103953.

[21] D.G. Aggelis, S. Verbruggen, E. Tsangouri, T. Tysmans, D. van Hemelrijck, Characterization of mechanical performance of concrete beams with external reinforcement by acoustic emission and digital image correlation, Constr. Build. Mater. 47 (2013) 1037–1045, https://doi.org/10.1016/J.CONBUILDMAT.2013.06.005.

[22] E. Vandecruys, C. Martens, C.V.A.N. Steen, H. Nasser, G. Lombaert, E. Verstrynge, Preliminary results on acoustic emission and vibration-based monitoring of locally corroded reinforced concrete beams (2022) 1–10.

[23] X. Zhou, W. Shan, J. Liu, J. Li, Fracture characterization of composite slabs with different connections based on acoustic emission parameters, Struct. Control Health Monit. 28 (2021) 1–15, https://doi.org/10.1002/stc.2703.

[24] N.A.A.S. Bahari, S. Shahidan, S.R. Abdullah, N. Ali, S.S. Mohd Zuki, M.H. W. Ibrahim, M.A. Rahim, Crack classification in concrete beams using AE parameters, IOP Conf. Ser.: Mater. Sci. Eng. 271 (2017) 012090.

[25] M.K. Elbatanouny, P.H. Ziehl, A. Larosche, J. Mangual, F. Matta, A. Nanni, Acoustic emission monitoring for assessment of prestressed concrete beams, Constr. Build. Mater. 58 (2014) 46–53, https://doi.org/10.1016/j.conbuildmat.2014.01.100.

[26] P.R. Prem, A.R. Murthy, M. Verma, Theoretical modelling and acoustic emission monitoring of RC beams strengthened with UHPC, Constr. Build. Mater. 158 (2018) 670–682, https://doi.org/10.1016/J.CONBUILDMAT.2017.10.063.

[27] Z. Wang, P. Willett, P.R. Deaguiar, J. Webster, Neural network detection of grinding burn from acoustic emission, Int J Mach Tool Manu 41 (2001) 283–309, https://doi.org/10.1016/S0890-6955(00)00057-2.

[28] A. Haug, F. Zachariassen, D. van Liempd, The costs of poor data quality, Journal of Industrial Engineering and Management 4 (2011), https://doi.org/10.3926/jiem.2011.v4n2.p168-193.

[29] V. Soltangharaei, R. Anay, L. Assi, M. Bayat, J.R. Rose, P. Ziehl, Analyzing acoustic emission data to identify cracking modes in cement paste using an artificial neural network, Constr. Build. Mater. 267 (2021), 121047, https://doi.org/10.1016/j.conbuildmat.2020.121047.

[30] S.D. R Monika, Deep Neural Networks on Acoustic Emission in Stress Corrosion Cracking., in: In International Conference on Artificial Intelligence and Sustainable Engineering, 2022: p. (pp. 151-167).

[31] X. Tan, P. Guo, X. Zou, Y. Bao, Buckling detection and shape reconstruction using strain distributions measured from a distributed fiber optic sensor, Measurement 200 (2022), 111625, https://doi.org/10.1016/J.MEASUREMENT.2022.111625.

[32] Z. Wang, F. Chegdani, N. Yalamarti, B. Takabi, B. Tai, M. el Mansori, S. Bukkapatnam, Acoustic emission characterization of natural fiber reinforced plastic composite machining using a random forest machine learning model, Journal of Manufacturing Science and Engineering Transactions of the ASME 142 (2020), https://doi.org/10.1115/1.4045945.

[33] C. Bhat, M.R. Bhat, C.R.L. Murthy, Acoustic emission characterization of failure modes in composites with ANN, Compos. Struct. 61 (3) (2003) 213–220.

[34] D. Li, K.S.C. Kuang, C.G. Koh, Fatigue crack sizing in rail steel using crack closure-induced acoustic emission waves, Meas. Sci. Technol. 28 (6) (2017) 065601.

[35] X. Zhang, N. Feng, Y. Wang, Y.i. Shen, Acoustic emission detection of rail defect based on wavelet transform and Shannon entropy, J. Sound Vib. 339 (2015) 419–432.

[36] A. Ebrahimkhanlou, S. Salamone, Single-Sensor Acoustic Emission Source Localization in Plate-Like Structures Using Deep Learning †, (n.d.). https://doi.org/10.3390/aerospace5020050.

[37] S. Grigg, R. Pullin, M. Pearson, D. Jenman, R. Cooper, A. Parkins, C.A. Featherston, Development of a low-power wireless acoustic emission sensor node for aerospace applications, Struct. Control Health Monit. 28 (4) (2021).

[38] A. Meserkhani, S.M. Jafari, A. Rahi, Experimental comparison of acoustic emission sensors in the detection of outer race defect of angular contact ball bearings by artificial neural network, Measurement (Lond). 168 (2021) 108198.

[39] G. Ma, Q. Du, Structural health evaluation of the prestressed concrete using advanced acoustic emission (AE) parameters, Constr. Build. Mater. 250 (2020), 118860, https://doi.org/10.1016/j.conbuildmat.2020.118860.

[40] L.i. Ai, V. Soltangharaei, M. Bayat, M. Van Tooren, P. Ziehl, Detection of impact on aircraft composite structure using machine learning techniques, Meas. Sci. Technol. 32 (8) (2021) 084013.

[41] Y. Hassan Ali, R. Abd Rahman, R.I. Raja Hamzah, Acoustic emission signal analysis and artificial intelligence techniques in machine condition monitoring and fault diagnosis: A review, Jurnal Teknologi (Sciences and Engineering) 69 (2014) 121–126. https://doi.org/10.11113/jt.v69.3121.

[42] S.J.S. Hakim, H.A. Razak, Modal parameters based structural damage detection using artificial neural networks - A review, Smart Struct. Syst. 14 (2) (2014) 159–189.

[43] L.K. Hansen, P. Salamon, Neural network ensembles, IEEE Trans. Pattern Anal. Mach. Intell. 12 (10) (1990) 993–1001.

[44] S. Yang, A. Browne, Neural network ensembles: combining multiple models for enhanced performance using a multistage approach, Expert. Syst. 21 (5) (2004) 279–288.

[45] H. Drucker, R. Schapire, P. Simard, Boosting performance in neural networks, Intern J Pattern Recognit Artif Intell. 07 (04) (1993) 705–719.

[46] H. Schwenk, Y. Bengio, Adaboosting neural networks: Application to on-line character recognition, Lecture Notes in Computer Science (Including Subseries Lecture Notes in Artificial Intelligence and Lecture Notes in Bioinformatics) (1997), https://doi.org/10.1007/bfb0020278.

[47] H. Sarmadi, A. Entezami, B. Saeedi Razavi, K.V. Yuen, Ensemble learning-based structural health monitoring by Mahalanobis distance metrics, Struct. Control Health Monit. 28 (2021), https://doi.org/10.1002/stc.2663.

[48] B.P. Duong, J.M. Kim, Pipeline fault diagnosis using wavelet entropy and ensemble deep neural technique, Lecture Notes in Computer Science (Including Subseries Lecture Notes in Artificial Intelligence and Lecture Notes in Bioinformatics) (2018), https://doi.org/10.1007/978-3-319-94211-7_32.

[49] L. Ai, V. Soltangharaei, P. Ziehl, Developing a heterogeneous ensemble learning framework to evaluate Alkali-silica reaction damage in concrete using acoustic emission signals, Mech. Syst. Sig. Process. 172 (2022), 108981, https://doi.org/10.1016/J.YMSSP.2022.108981.

[50] J. Li, U. Dackermann, Y.-L. Xu, B. Samali, Damage identification in civil engineering structures utilizing PCA-compressed residual frequency response functions and neural network ensembles, Struct. Control Health Monit. 18 (2) (2011) 207–226.

[51] ASTM, Astm D6272 Standard Test Method for Flexural Properties of Unreinforced and Reinforced Plastics and Electrical Insulating Materials by Four-Point Bending, Annual Book of ASTM Standards. 02 (2017).

[52] AASHTO, The Manual for Bridge Evaluation, 2011.

[53] L. Ai, V. Soltangharaei, M. Bayat, B. Greer, P. Ziehl, Source localization on large-scale canisters for used nuclear fuel storage using optimal number of acoustic

emission sensors, Nucl. Eng. Des. 375 (2021), 111097, https://doi.org/10.1016/J.NUCENGDES.2021.111097.

[54] B. Yegnanarayana, Artificial neural networks for pattern recognition, Sadhana 19 (2) (1994) 189–238.

[55] H. Adeli, Neural networks in civil engineering: 1989–2000, Computer-Aided Civil and Infrastructure Engineering 16 (2) (2001) 126–142.